AIAA 92-0316

An Analytical and Computational Investigation of Shock-Induced Vortical Flows

Joseph Yang, Toshi Kubota, and Edward E. Zukoski
California Institute of Technology
Pasadena, CA

30th Aerospace Sciences Meeting & Exhibit
January 6-9, 1992 / Reno, NV

AN ANALYTICAL AND COMPUTATIONAL INVESTIGATION OF SHOCK-INDUCED VORTICAL FLOWS

Joseph Yang*, Toshi Kubota**, and Edward E. Zukoski†
California Institute of Technology
Pasadena, California

Abstract

Interaction of a shock wave with a jet of light gas surrounded by an ambient heavy gas generates vorticity around the perimeter of the jet. This rolls the jet into a pair of counterrotating, finite-core size vortices. The canonical problem is the two-dimensional, unsteady interaction in a finite channel. The dynamics of the vortex pair are controlled by the incident shock strength, the light/heavy gas density ratio, and the channel spacing. Analytical expressions are derived which describe the strength and motion of the vortex pair as a function of these parameters. Numerical simulations show good agreement with these models. Various perturbations on the single jet flow are investigated with the goal of destabilizing the vortex pair and further enhancing the mixing. Single jet shape perturbations are relatively ineffective. However, an array of jets can dramatically increase the mixing. Another effective method is to form a reflected shock. Finally, an analogy to the corresponding three-dimensional, steady flows is demonstrated both qualitatively and quantitatively. This allows an understanding of the dynamics and mixing of the two-dimensional, unsteady flows to be directly applied to three-dimensional, steady flows typical of SCRAMJET designs.

Introduction

The motivation for the study of shock-induced vortical flows is the combustion of fuel and oxidizer in a supersonic combustion ramjet, such as the proposed National Aerospace Plane. In such a vehicle, supersonic air flow into the combustion chamber limits the residence time to only a few milliseconds. This imposes a severe requirement for rapid and efficient mixing of fuel and oxidizer.

Marble, *et al.*[4,5] proposed the mechanism of shock-induced vorticity generation as a possible means for achieving this mixing. In particular, they showed that the interaction of a jet of light gas would generate vorticity around the perimeter of the jet. This vorticity would then cause the jet to roll up at its front and rear edges, stirring and mixing the light gas with the ambient heavy gas (Figure 1). They also qualitatively argued that the three-dimensional (3-D), steady flow in an actual injector design should be analogous to a two-dimensional (2-D), unsteady flow which is often more conveniently studied, either experimentally or computationally. In the 3-D flow, an oblique shock passes vertically upward through the jet as it moves downstream. In the analogous 2-D flow (Figure 2), a normal shock propagates through a planar region of light gas as a function of time, and the gas rolls up at its upper and lower edges.

The present work is an analytical and computational investigation of the shock-induced vortical flow in the 2-D, unsteady case. Two broad aims can be stated. One is to develop a comprehensive description of the canonical problem. The problem is investigated computationally, by solution of the governing differential equations with various initial conditions. This establishes a qualitative understanding of the important flow features, as well as quantifying the behavior over a range of flow parameters. Then, independently of the computations, analytical models for the flow are developed and compared against the computations. This provides the ability to predict key features of the flow without having to perform expensive and time-consuming computations.

The second aim is to characterize the mixing of shock-induced vortical flows, for the canonical problem and also for variations on the canonical problem that represent configurations more appropriate to a real flow. Computations are performed for both single jet shape perturbations and multiple jet geometrical variations. This gives a qualitative understanding of how each case differs from the canonical flow. Finally, a means of characterizing the mixing is developed and used to make quantitative comparisons.

The Computational Algorithm

The conservation equations for continuity, momentum, energy, and species are integrated on a Cray Y-MP computer using LCPFCT,[6] an explicit, Eulerian finite-difference, flux-corrected transport algorithm.

The flow is initialized by specifying density, velocity, pressure, and concentration fields for the jet, the ambient fluid surrounding the jet, and the normal shock wave impinging from left to right. The jet is initialized using a similarity solution for the mixing layer at the edge of an axisymmetric jet, at a plane several diame-

* Presently Associate Research Engineer, Shell Development Company; Member, AIAA
** Professor Emeritus of Aeronautics; Member, AIAA
† Professor of Jet Propulsion and Mechanical Engineering; Member, AIAA

ters downstream from the nozzle.

During the computation, the domain is moved in time to track the developing vortex pair. Full details of the computational technique are given in Reference 11.

Computations of the Canonical Problem

Qualitative Description

Consider again the interaction shown in Figure 2. The inviscid vorticity equation can be written as

$$\frac{D\underline{\omega}}{Dt} = \frac{1}{\rho^2}\,(\underline{\nabla}\rho \times \underline{\nabla}p) + \ldots,$$

giving a rate of generation of vorticity proportional to the cross product of the density and pressure gradients. As the shock wave passes over the jet, vorticity is deposited around the circumference of the jet, as shown in Figure 2(b). The density gradient, due to the density jump at the circumference of the jet, is everywhere radially outward. The pressure gradient, due to the pressure jump across the shock, points upstream. Where the pressure gradient is perpendicular to the density gradient ($\theta = \pm\pi/2$), the vorticity is maximum. Where the two gradients are parallel ($\theta = 0, \pi$), the vorticity is zero. Elsewhere, the vorticity is intermediate.

The deposited vorticity will initially cause the jet to roll up into a kidney-shaped structure, as shown in Figure 2(c). As time goes on, the vorticity will coalesce and the structure will evolve toward a vortex pair with finite core size, as shown in Figure 2(d).

It will be more convenient to present results in nondimensional variables, indicated by an overbar. All lengthscales are normalized by R_0, the initial radius of the jet, all velocities are normalized by c_1, the speed of sound in the ambient fluid ahead of the shock, and all times are normalized by R_0/c_1. Densities and pressures are normalized by ρ_1 and p_1, the values in the ambient fluid ahead of the shock.

Figure 3 shows density contour plots from a computation of a M=1.1 incident shock with an isolated single circular helium jet in air (light/heavy gas density ratio $\overline{\rho}_L/\overline{\rho}_H = 0.138$). Notice that, in the nondimensional variables defined above, the radius of the jet is unity. The development of the structure verifies the predictions of Figure 2. At $\overline{t} = 0^+$, the shock wave passes over the jet and vorticity is deposited around the circumference. It is the self-induced motion from the vorticity distribution that drives the development of the structure. At $\overline{t} = 10$, the circular section deforms to a kidney shaped structure. At $\overline{t} = 30$ the contours begin to coalesce into the characteristic closed shape of a vortex core, and this pinches off a region of lower vorticity fluid as an upstream tail. At the downstream end, a well-defined thin filament connects the upper half plane vortex with its lower half plane image. At $\overline{t} = 40$, note the emergence of smooth closed contours in the centers of the vortices, indicating stabilization. At $\overline{t} = 50$, each core experiences a strong horizontal induced velocity from its image. Thus the cores move downstream much more rapidly than the tails, which stretch upstream as they trail behind. The remainder of the time history shows continued development toward a steady-state vortex pair with trailing low-vorticity tails.

Quantitative Description

The overall fluid mechanical behavior, *i.e.*, strength and motion of the vortex pair, may be determined from the computations as follows.

Consider again the M=1.1, $\overline{\rho}_L/\overline{\rho}_H = 0.138$ flow of Figure 3. The circulation about one of the vortical structures is shown in Figure 4(a). It is calculated by evaluating the integral

$$\overline{\Gamma} \equiv \oint \underline{\overline{u}} \cdot d\underline{\overline{x}}$$

around a rectangular contour coincident with the upper-half-plane of the flow field. The circulation rises rapidly as the shock passes through the jet, the peak (at $\overline{t} = 4$) corresponding to the point where the transmitted shock is just exiting the downstream end of the jet. Thereafter, there are some very small oscillations due to various reflected and transmitted waves, but the changes due to these waves are small and may be neglected.

The $\overline{x}$-trajectory is shown in Figure 4(b). This is defined as the center of mass fraction, in the $\overline{x}$-direction, relative to the moving fluid behind the shock, *i.e.*,

$$\overline{x}_{cmf} \equiv \frac{\int \overline{x} f \; d\overline{A}}{\int f \; d\overline{A}}.$$

There is a small early time dip just after the shock passes over the jet, when the still stationary jet appears to move backwards relative to the moving ambient fluid. However, the deposited vorticity soon accelerates the structure to a velocity faster than the ambient fluid. Throughout the development of the vortex pair, the trajectory is very steady, the velocity of translation $\overline{U} \equiv d\overline{x}_{cmf}/d\overline{t}$ being essentially constant.

The $\overline{y}$-trajectory (or half-spacing of the vortex pair) is shown in Figure 4(c). This is defined as the center of mass fraction, in the $\overline{y}$-direction, of the upper half plane portion of the structure, *i.e.*,

$$\overline{y}_{cmf} \equiv \frac{\int \overline{y} f \; d\overline{A}}{\int f \; d\overline{A}}.$$

The trajectory shows a rapid initial increase as the lobes first develop ($\overline{t}$=0 to 20). After this point, there are small fluctuations as the vortex continues to stabilize, but $\overline{y}_{cmf}$ asymptotically approaches a steady-state value, denoted by $\overline{y}_\infty$.

Computations were also performed for circular jets with different shock strengths and light/heavy gas density ratios. As the shock strength was increased or the light/heavy gas density ratio was decreased, the structure developed more rapidly and was more nearly an ideal vortex pair. Steady-state values of circulation, half-spacing, and velocity for the family of canonical flows are summarized in Table 1. In some cases, the

computation was not carried out long enough for some parameters to reach steady-state conditions.

M	$\overline{\rho}_L/\overline{\rho}_H$	$\overline{\Gamma}$	$\overline{y}_\infty$	$\overline{U}$
1.05	0.138	0.24	0.72	0.018
1.1	0.138	0.45	0.75	0.033
1.2	0.138	0.72	0.82	0.054
1.5	0.138	0.97	1.00	0.063
2.0	0.138	1.20	1.00	0.070
1.1	0.354	0.272	0.82	0.0195
1.1	0.569	0.162	Not Steady	
1.1	0.785	0.075	Not Steady	
2.0	0.354	0.765	1.20	0.0300
2.0	0.569	0.448	1.20	0.0193
2.0	0.785	0.205	Not Steady	

Table 1 - $\overline{\Gamma}$, $\overline{y}_\infty$, and $\overline{U}$ for the canonical flows

Analytical Models for the Canonical Problem

Circulation

The strength of the vortex pair, throughout the development from post-shock roll-up to late-time steady-state, is completely characterized by a single value of $\overline{\Gamma}$. Since this circulation is determined only by the initial interaction, it should be a function of only the shock strength and the density ratio. Various authors have attempted to develop models to describe this relationship.

The problem was first considered by Rudinger and Somers,[9] using an impulsive motion analysis. Although they did not derive an explicit formula for circulation, their results may be manipulated to give

$$\overline{\Gamma} = \frac{8}{\pi}\,\overline{y}_\infty\,\overline{v}_2\left(\frac{1-\overline{\rho}_L/\overline{\rho}_H}{1+\overline{\rho}_L/\overline{\rho}_H}\right).$$

$\overline{v}_2$ is the velocity behind the shock, which is purely a function of M. Note that the formula predicts a dependence on the vortex half-spacing, $\overline{y}_\infty$. Rudinger and Somers did not measure circulation or vortex core spacing, so a direct comparison between their model and their results can not be made.

Picone, *et al.*[7,8] analytically integrated the vorticity equation to give

$$\overline{\Gamma} = 2\,\overline{v}_2\left(\frac{\overline{v}_2}{2M}-1\right)\ln\left(\frac{\overline{\rho}_L}{\overline{\rho}_H}\right).$$

However, their own computations, for the case of a helium cylinder in air, showed that their model overpredicts the computed circulation by a factor of two.

Most recently, using simple one-dimensional gasdynamics, Hendricks and Marble[2] derived a set of coupled, nonlinear equations that could be solved numerically for $\overline{\Gamma}$ as a function of M and $\overline{\rho}_L/\overline{\rho}_H$. The disadvantages of this method are that the physical dependences can not be easily visualized, and that the equations are tedious, although straightforward, to solve numerically. Hendricks and Marble showed good agreement between their model and their computations for two low Mach number He/air cases.

One would like to have a model that is both accurate and easy to use. The present derivation is as follows. Consider a cross section through an axisymmetric circular jet, as shown in Figure 5. The radius of the jet is R_0, and the interface is idealized as a sharp step discontinuity in density. The light jet gas has density ρ_L and the heavy gas has density ρ_H $(=\rho_1)$. A shock wave of strength M approaches from left to right. The density and pressure ratios across the shock wave ($(\ )_1$ = ahead and $(\ )_2$ = behind) are

$$\frac{\rho_2}{\rho_1} = \frac{(\gamma_1+1)M^2}{(\gamma_1-1)M^2+2},$$

and

$$\frac{p_2}{p_1} = 1+\left(\frac{2\gamma_1}{\gamma_1+1}\right)(M^2-1).$$

The vorticity production term of the vorticity equation is

$$\frac{D\underline{\omega}}{Dt} = \frac{1}{\rho^2}(\underline{\nabla}\rho\times\underline{\nabla}p)+\cdots.$$

The vorticity is perpendicular to the plane of the jet, $\underline{\omega} = \omega\hat{e}_z$. Integrating the vorticity equation for ω gives

$$\begin{aligned}\omega &= \int_0^\infty \frac{1}{\rho^2}\,|\underline{\nabla}\rho\times\underline{\nabla}p|\;dt\\ &= \frac{1}{\rho^2}\int_0^\infty |\underline{\nabla}\rho||\underline{\nabla}p|\;sin\theta\;dt\\ &= \frac{1}{\rho^2}\int_0^\infty \Delta\rho\;\delta(r-R_0)\;\Delta p\;\delta(x-V_s t)\;sin\theta\;dt\\ &= \frac{1}{V_s}\,\frac{\Delta\rho}{\rho}\,\frac{\Delta p}{\rho}\;sin\theta\;\delta(r-R_0).\end{aligned}$$

Having this expression for the vorticity, integrating over half the area of the jet gives the circulation:

$$\begin{aligned}\Gamma &\equiv \int\int \omega dA\\ &= \frac{1}{V_s}\,\frac{\Delta p}{\rho}\,\frac{\Delta\rho}{\rho}\int_0^\pi\int_0^\infty \delta(r-R_0)\;sin\theta\;r\;dr\;d\theta\\ &= \frac{2R_0}{V_s}\,\frac{\Delta p}{\rho}\,\frac{\Delta\rho}{\rho}.\end{aligned}$$

It is necessary to choose suitable values of ρ, one for the pressure term, and one for the density term. Since the pressure gradient is due to the shock, choose ρ_2 for the pressure term, and since the density gradient is across the interface, choose the average density at the interface, $(\rho_L+\rho_H)/2$, for the density term. The circulation then becomes

$$\Gamma = \frac{4R_0}{V_s}\,\frac{\Delta p}{\rho_2}\left(\frac{\Delta\rho}{\rho_L+\rho_H}\right).$$

Finally, nondimensionalize all lengths by R_0, all densities by ρ_1, all pressures by p_1, all velocities by c_1, and the circulation by R_0c_1. The circulation then becomes

$$\overline{\Gamma} = \frac{4}{\gamma_1 M}\left(\frac{\overline{\rho}_1}{\overline{\rho}_2}\right)\left(\frac{\overline{p}_2}{\overline{p}_1}-1\right)\left(\frac{1-\overline{\rho}_L/\overline{\rho}_H}{1+\overline{\rho}_L/\overline{\rho}_H}\right).$$

One can test this model against those described earlier, in predicting the computed circulation data of Table 1. The results are tabulated in Table 2, for the cases which were computed to steady state.

M	$\overline{\rho}_L/\overline{\rho}_H$	Comp. $\overline{\Gamma}$	Predicted $\overline{\Gamma}$(R-S)	$\overline{\Gamma}$(P-B)	$\overline{\Gamma}$(H-M)	$\overline{\Gamma}$(Yang)
1.05	0.138	0.240	0.113	0.310	0.196	0.228
1.1	0.138	0.450	0.230	0.584	0.376	0.412
1.2	0.138	0.720	0.483	1.056	0.699	0.690
1.5	0.138	0.970	1.339	2.113	1.455	1.130
2.0	0.138	1.200	2.410	3.402	2.338	1.420
1.1	0.354	0.272	0.159	0.318	0.239	0.260
2.0	0.354	0.765	1.824	1.787	1.415	0.896
1.1	0.569	0.162	0.098	0.172	0.144	0.150
2.0	0.569	0.448	1.049	0.969	0.863	0.515
1.1	0.785	0.075	0.038	0.074	0.069	0.066
2.0	0.785	0.205	0.461	0.417	0.453	0.226

Table 2 - Computed and predicted $\overline{\Gamma}$

The present ('Yang') model appears to give the best result, with about 15% maximum deviation between predicted and computed values. The Hendricks and Marble ('H-M') model works reasonably well, but the Rudinger and Somers ('R-S') and Picone and Boris ('P-B') models are as much as a factor of 2 in error.

Characteristic Time

One would also like to have a model to describe the characteristic time for development of a flow. This would provide the ability to make temporal comparisons between different flows within the same family. For example, given a full description of the time-dependent flow for specific values of M and $\overline{\rho}_L/\overline{\rho}_H$, one could predict the times for equivalent stages of development if either of these initial conditions were changed.

A characteristic time for the interaction can be formulated as

$$\tau \equiv \frac{H\ W}{\Gamma} ,$$

where H is a characteristic height, W is a characteristic width, and Γ is the circulation. For H, one takes R_0, the vertical dimension, and for L, one takes $(\rho_1/\rho_2)R_0$, the horizontal dimension just after the shock has passed (the factor (ρ_1/ρ_2) accounts for the streamwise compression due to the shock). Therefore,

$$\tau = \frac{\rho_1}{\rho_2}\ \frac{R_0^2}{\Gamma} .$$

Nondimensionalizing and substituting the previous expressions for $\overline{\Gamma}$ and ρ_2/ρ_1 gives

$$\overline{\tau} = \left(\frac{\gamma_1+1}{8}\right)\left(\frac{M}{M^2-1}\right)\left(\frac{1+\overline{\rho}_L/\overline{\rho}_H}{1-\overline{\rho}_L/\overline{\rho}_H}\right) .$$

This model can be tested against the data from the computations. For example, the model predicts that $\overline{\tau}(M = 1.1, \overline{\rho}_L/\overline{\rho}_H = 0.785)\ /\ \overline{\tau}(M = 1.1, \overline{\rho}_L/\overline{\rho}_H = 0.569) = 2.29$, so that a M=1.1, $\overline{\rho}_L/\overline{\rho}_H = 0.785$ flow at $\overline{t}$=91.6 and a M=1.1, $\overline{\rho}_L/\overline{\rho}_H = 0.569$ flow at $\overline{t}$=40 should represent equivalent stages of development. Times $\overline{t}$ = 90 and 40 are shown in Figure 6. The agreement is quite good. Other comparisons may be found in Reference 11.

Normalized Velocity

The late-time structure resulting from the interaction of a shock wave and a single jet is essentially a vortex pair with finite core size, in a channel of finite height. Relative to the ambient fluid, the structure moves downstream with a velocity due to the induced motion of each vortex by the other.

The simplest model for the motion of a vortex pair is the potential flow of a point vortex pair in an unbounded domain, which predicts the normalized velocity to be $\overline{U}\overline{y}_\infty/\overline{\Gamma} = 1/(4\pi)$. This model would be an accurate representation of the velocity in the simultaneous limits of core size tending toward zero and channel spacing tending toward infinity. Qualitatively, it is clear that this model represents an upper limit for the velocity that can be realized in an actual flow. As either the core size or channel spacing becomes finite, the velocity must decrease below $\overline{U}\overline{y}_\infty/\overline{\Gamma} = 1/(4\pi)$.

First consider the effect of channel spacing alone. This problem consists of a pair of point vortices in a bounded domain. The vortex spacing is $2\overline{y}_\infty$ and the channel spacing is $2\overline{h}$. The solution is a superposition of the point vortex solution, treating each wall or horizontal line of symmetry as a line of reflection. The result[11] is

$$\frac{\overline{U}\overline{y}_\infty}{\overline{\Gamma}} = \frac{1}{4}\ \frac{\overline{y}_\infty}{\overline{h}}\ ctg\left(\pi\frac{\overline{y}_\infty}{\overline{h}}\right) .$$

Next consider the effect of finite core size alone. The model for this flow is a vortex pair with constant vorticity inside a finite core, in an unbounded domain. The simplifying assumption of constant vorticity, although not realizable in an actual flow, should be a reasonable approximation when the vortex core is large compared to the vorticity gradient at the edge of the region.

The solution takes the form of a perturbation analysis, with perturbation parameter $\epsilon \equiv \overline{R}/\overline{y}_\infty$. The unperturbed flow is a pair of circular vortices with initial radii $\overline{R}$. The flow is assumed to be incompressible with uniform density throughout. The vortices are characterized by $\overline{\omega}$ = constant, $\overline{\Gamma}$ = constant, $\overline{A}$ = constant, and therefore, $\overline{R} \equiv (\overline{A}/\pi)^{1/2}$ = constant.

The boundary is allowed to deform subject to the kinematical condition that the vortex pair moves, without change of spacing, downstream at a constant velocity. Both the boundary shape and the translational velocity are expressed as perturbation expansions in ϵ. These conditions introduce one constraint equation and two undetermined expansions involving unknown coefficients times powers of ϵ.

The boundary conditions at the vortex boundary require continuity of both normal and tangential veloci-

ties there. In addition, the normal velocity of each point on the boundary must satisfy the constraint of steady translational motion at the velocity of the vortex pair. These conditions introduce three more constraint equations.

The velocities inside and outside the boundary are also expanded in the perturbation parameter ϵ. Each velocity field is a superposition of self-induced velocities and velocities induced by the other vortex. The lowest order 'inner, self' contribution is due to a solid body rotation. The lowest order 'inner, other' contribution is due to a point vortex. The lowest order 'outer, self' and 'outer, other' terms are due to a point vortex. Higher order terms, which involve corrections for deformation of boundary shape, are distinguished as 'inner' and 'outer,' but not as 'self' and 'other.' It is convenient to express the complex velocity $\overline{u}-i\overline{v}$ is an analytic function of the complex variable $\overline{z}=\overline{x}+i\overline{y}$, so that the 'correction' velocities may be expressed as appropriate Laurent series in $\overline{z}$. The 'inner' velocity is described by a series having only positive powers of $\overline{z}$, while the 'outer' velocity is described by a series having only negative powers of z. These conditions introduce two more undetermined expansions.

At this point, there are four equations and four expansions, so the unknown coefficients in the expansions may be determined, term-by-term, by powers of epsilon. The algebraic manipulations are tremendous, especially at higher orders. To 6-th order, the normalized velocity is given by[11]

$$\frac{\overline{U}\overline{y}_\infty}{\overline{\Gamma}} = \frac{1}{4\pi} - \frac{1}{32\pi}\left(\frac{\overline{R}}{\overline{y}_\infty}\right)^4 + O\left(\frac{\overline{R}}{\overline{y}_\infty}\right)^6 .$$

For convenience in the derivation of this solution, the density was assumed uniform everywhere. Such is not the case in the actual flow. For consistency with the assumption of piecewise constant vorticity, one should at least model the density as piecewise constant: low inside the vortex core and high outside the vortex core. However, it can be shown[11] that the uniform density solution gives the same result for normalized velocity as in the case of piecewise constant density.

Combining the two previous results gives an expression for normalized velocity that includes the effect of both vortex core size and channel spacing. To lowest order, the result is

$$\frac{\overline{U}\overline{y}_\infty}{\overline{\Gamma}} \approx \frac{1}{4\pi}\,\frac{\pi\overline{y}_\infty}{\overline{h}}\,\left[ctg\left(\frac{\pi\overline{y}_\infty}{\overline{h}}\right)\right]\left[1-\frac{1}{8}\left(\frac{\overline{R}}{\overline{y}_\infty}\right)^4\right] .$$

One can test this model using data from the computations listed in Table 1. The size of the vortex core,

$$\overline{R} \equiv \sqrt{\frac{\overline{A}}{\pi}},$$

is based on the mass fraction-weighted area,

$$\overline{A} \equiv \int f\, d\overline{A}.$$

Table 3 lists the computed and predicted normalized velocities for the canonical flows.

M	$\overline{\rho}_L/\overline{\rho}_H$	$\overline{R}/\overline{y}_\infty$	$\overline{y}_\infty/\overline{h}$	Computed $\overline{U}\overline{y}_\infty/\overline{\Gamma}$	Predicted $\overline{U}\overline{y}_\infty/\overline{\Gamma}$
1.05	0.138	1.054	0.180	0.0540	0.0600
1.1	0.138	0.987	0.188	0.0550	0.0618
1.1	0.354	0.898	0.205	0.0588	0.0627
1.2	0.138	0.881	0.200	0.0600	0.0636
1.5	0.138	0.669	0.238	0.0617	0.0626
2.0	0.138	0.547	0.250	0.0583	0.0618
2.0	0.354	0.456	0.300	0.0471	0.0542
2.0	0.569	0.444	0.300	0.0517	0.0542

Table 3 - Computed and predicted $\overline{U}\overline{y}_\infty/\overline{\Gamma}$

The model slightly overpredicts the computed normalized velocities, but the trends are well reproduced. For example, Figure 7 shows the expected behavior for a family of fixed density ratio flows: (a) as M increases, the vortices become more compact so their velocity increases; (b) at the same time, they approach the channel walls so their velocity decreases; (c) both effects together lead to a slightly concave downward dependence on M. This behavior is confirmed by both the model and the computations for the case $\overline{\rho}_L/\overline{\rho}_H = 0.138$ (Figure 8).

In these computations, the effects of vortex spacing/channel spacing and vortex size/vortex spacing are implicit in the variation of M and $\overline{\rho}_L/\overline{\rho}_H$. Computations were also performed[9] for explicit variations in channel spacing, and, again, the model predicted the normalized velocities quite accurately.[11]

Variations on the Canonical Problem

Up to this point, only the case of a single shock wave interacting with a single, isolated, circular jet has been considered. Although this canonical problem is convenient for studying the basic physics of the interaction, it is not representative of flows that would occur in real devices. For example, real jets may be noncircular in shape. Also, there may be multiple shock waves in the domain. Finally, technological applications will probably involve arrays of multiple jets as opposed to a single jet.

Single Jet Shape Perturbations

Two families of perturbations to the single jet shape were computed: elliptical cross-sectional shape and circular shape with sinusoidal instabilities at the circumference of the jet. The qualitative behavior of these flows were essentially the same as the circular jet: a dominant, stable vortex pair with trailing tails of low-vorticity material. There were minor differences in the details of the flow, particularly in the size and character of the tails, but the basic flow pattern was unchanged. Details may be found in Reference 11.

Reflected Shock Interactions

Another possibility, especially in a closed domain, is that a reflected shock may reflect from the end wall and interact with the vortex pair formed by the incident shock. For example, Figure 9 shows the interaction of a late-time reflected normal shock formed by an incident M=2 shock in an $\overline{\rho}_L/\overline{\rho}_H = 0.138$ flow.

The interaction of the reflected shock with the vortex core results in baroclinic generation of vorticity similar, but opposite in sense, to that produced by the incident shock. For example, consider the upper half plane. The most important feature is the strong vorticity initially present in the vortex core. In the absence of this vorticity, the approximately circular core would behave like the single circular jet considered previously. Vorticity deposited in the outer half of the core would develop into a clockwise vortex, and vorticity deposited in the inner half would develop into a counterclockwise vortex. These vortices would convect upstream relative to the ambient velocity because of their mutually induced velocities. In this case, however, the strong counterclockwise initial vorticity suppresses the outer half's development and enhances the inner half's development. The result is the formation of an asymmetrical vortex pair, consisting of a small, clockwise outer vortex and a large, counterclockwise inner vortex. The strong inner vortex induces a counterclockwise downward and inward motion of the weak outer vortex. The weak outer vortex induces negligible motion of the inner vortex. Thus the overall motion is a counterclockwise rotation of the weak outer vortex about the strong inner vortex.

Multiple Jet Arrays

Families of multiple jet configurations were also computed. The most effective configuration was found to be a horizontal pair of jets. For example, Figure 10 shows a M=1.1, $\overline{\rho}_L/\overline{\rho}_H = 0.138$ flow with an initial center-to-center jet spacing of 4 radii. At early times, each jet develops into a vortex pair similar to the isolated single circular jet case. But as time goes on, the vortex pairs interact, in a manner that can be predicted from simple induced motion considerations. Figure 11(a) is a schematic of the vortex cores. The single arrows illustrate the induced motion of each core due to all the others. For example, consider the UHP downstream core. It experiences a rightward velocity due to its LHP neighbor, an upward velocity due to its upstream UHP neighbor, and a rightward and downward velocity due to its upstream LHP neighbor. The net velocity, shown as a double arrow, is upward and rightward. Similarly, the net velocity of the UHP upstream core is downward and rightward. As the downstream cores move apart, they induce in each other smaller downstream velocities, and the pair decelerates. Similarly, as the upstream cores move closer together, they induce in each other larger downstream velocities, and the pair accelerates. Thus, the upstream vortex pair is entrained into the downstream one. Figure 11(b) shows the induced motion of the tail of the downstream UHP structure, due to the two UHP vortex cores. Its net motion is upward and to the left. Thus, the tail is pulled up and around the outer edge of the upstream UHP vortex core.

Other configurations were also studied, including vertical jet pairs, horizontal jet trios, and equilateral jet trios. Full details may be found in Reference 11.

Applications to Supersonic Combustion

Mixing Measure

The previous chapter presented qualitative discussions of the fluid mechanics of a number of variations on the canonical flow. These flows are of interest insofar as they may be used to enhance the mixing of fuel and oxidizer in an application such as supersonic combustion. Thus it is necessary to have a quantitative basis for comparing their mixing efficiencies.

One may think of mixing as a two-step process, as shown in Figure 12. The first step, stretching, is a necessary precursor to the second step, diffusion, because it is through gradient intensification that diffusive effects become important. Finite grid numerical simulations can accurately model kinematic effects such as stretching, but not molecular effects such as diffusion. When using numerical simulations, it is possible to measure mixing only indirectly, through the kinematics of the stretching precursor.

Batchelor[1] investigated the effect of homogeneous turbulence on material elements of fluid, and found the best achievable stretching rate to be exponential. More recently, other investigators have found that exponential stretching is also possible, at least locally, in essentially inviscid two-dimensional unsteady or three-dimensional steady flows[3]. In expectation of this possibility, one can define a specific stretching rate as

$$\frac{1}{\overline{L}}\frac{D\overline{L}}{D\overline{t}} = \frac{D}{D\overline{t}}\,[ln(\overline{L})],$$

and study the approach to exponential stretching as evidenced by the asymptotic behavior of this quantity as a function of time. $\overline{L}$ is the length of a material element following the fluid, and is taken to be a particular mass-fraction level of interest.

This choice of mass-fraction level is guided by flows of technological interest. Since the application of mixing is combustion, imagine a flow where the light gas is hydrogen, and the heavy gas is air, so that the balanced chemical equation is

$$2H_2 + (3.76N_2 + O_2) \rightarrow 3.76N_2 + 2H_2O$$

The stoichiometric fuel mass fraction is then found to be

$$f_s = \frac{2(2)}{2(2) + 3.76(28) + 2(16)} = 0.028.$$

The anticipated technological application for shock-induced mixing is, of course, the National Aerospace Plane, which will carry an excess of hydrogen, beyond

stoichiometric conditions, for cooling the structure in flight. Assuming a surplus on the order of 50%, this suggests that the actual fuel mass fraction will be

$$f \approx 1.5 f_s = 1.5(0.028) = 0.042.$$

Rounding upward, it is appropriate to pick f=0.05 as the contour whose stretching rate is of interest.

In a purely kinematical flow, the length of any material element will continue to stretch indefinitely. However, in numerical simulations (and in real flows), such is not the case. At some point, the features of interest will be stretched thinner than the grid size, and there will be an abrupt drop in the length of the mass fraction level of interest as resolution is lost. Or, there may be a gradual decrease in the rate of stretching due to numerical dissipation (in a real flow, this would correspond to molecular diffusion, *i.e.*, real mixing). In any case, the quantitative reliability of numerical data beyond that point can not be guaranteed.

Thus, for a mixing measure, one can define a critical stretching rate as that rate which is achieved at the drop-off point. This represents the best level of stretching that is achieved in the flow, before resolution or diffusion losses become important. In almost all the cases, the plots of $D[\ln \bar{L}]/D\bar{t}$ show a nearly straight-line approach to this point, indicating that the global stretching can indeed be well represented by an exponential expectation.[11]

Stretching rates for the canonical flows are listed in Table 4.

M	$\bar{\rho}_L/\bar{\rho}_H$	$D[\ln \bar{L}]/D\bar{t}$
1.05	0.138	0.007
1.1	0.138	0.014
1.2	0.138	0.024
1.5	0.138	0.050
2.0	0.138	0.085
1.1	0.354	0.010
1.1	0.569	0.006
1.1	0.785	0.002
2.0	0.354	0.061
2.0	0.569	0.048
2.0	0.785	0.035

Table 4 - Stretching rates for the canonical flows

The stretching rate increases as either the density ratio is decreased or the shock strength is increased, as both factors lead to increased induced motions and thus higher stretching rates. Note that the increase in stretching rate is greatest in cases of low Mach number or high density ratio. For example, at M=1.1, decreasing the density ratio from 0.785 to 0.138 increases the stretching rate by a factor of 7, while at M=2, the increase is only 2.5. Similarly, at $\bar{\rho}_L/\bar{\rho}_H = 0.785$, increasing M from 1.1 to 2.0 increases the stretching rate by a factor of 17, while at $\bar{\rho}_L/\bar{\rho}_H = 0.138$, the increase is only a factor of 6.

Unfortunately, space limitations prohibit a complete tabulation of the stretching rates for all the flow variations described previously. Only the general trends are summarized below, as the full results may be found in Reference 11.

Perturbations to single jet shape did not increase the stretching rates beyond the corresponding circular jet flows of the same Mach number and light/heavy gas density ratio. Since the stretching rate does not change, the stretching itself may be maximized by simply choosing a cross-sectional shape which maximizes the deposited vorticity, *i.e.*, minimizes the development time. This suggests that the jet should be elongated in the direction of the flow, as this provides a larger distance for baroclinic vorticity generation through misalignment of the density and pressure gradients. For example, given a requirement for a certain jet area, an elliptical jet elongated in the streamwise direction would be preferable to a circular jet.

Variations in wall spacing also had no effect on the stretching rate. However, the sharper the initial interface, the better the stretching.

The interaction of a reflected shock with the vortex pair produced by an incident shock caused was highly effective in increasing the stretching rate. For example, for the flow of Figure 9, the stretching rate was 0.165. This is a 94% increase in the stretching rate over the corresponding canonical flow. It was also found that the earlier the reflected shock hit, the better the increase in mixing.

Multiple jet arrays also increased the stretching rate, but not as much as the reflected shock. In general, the closer the jets initially, the better the increase in stretching rate. The most effective configuration was horizontal jet pairs. For example, for the flow of Figure 10, the stretching rate was 0.018, or 29% higher than the corresponding canonical flow.

The next most effective configuration was vertical jet pairs. Horizontal jet trios and equilateral jet trios were less effective, because the presence of a third body effectively slows the entrainment of one vortex pair into another.

In summary, given the requirement for a specified total jet area, one should use a several smaller jets rather than a single larger jet. Each jet should be elongated in the direction of shock passage. The jets should not form an evenly spaced array, but rather should be widely staggered in closely-spaced pairs, both horizontally and vertically. The light/heavy gas density ratio should be as small as possible, and the shock should be as strong as possible. Finally, one should strive to have reflected shocks (or other types of multiple shocks), as early as possible.

Analogy to 3 – D Steady Flows

Waitz[10] has computed a 3-D, steady flow in which the primary mechanism of mixing was also baroclinic generation of vorticity. His results are shown in Figure 13. A jet of helium is discharged from a rectangular injector, and flows downstream left to right. High speed air, passing over the downward sloping ramp on both sides of the injector, forms a shock wave at the abrupt transition to the combustor floor. As the shock wave

passes vertically upward through the jet, it generates vorticity in the manner described in Figure 1. The front and back edges of Waitz's flow are planes of symmetry between adjacent injectors.

Figure 14 shows a 2-D, unsteady computation corresponding to Waitz's flow. The geometries are matched in the following sense: the upper and lower walls of the 2-D flow correspond to the planes of symmetry in the 3-D flow, the left end of the 2-D flow is a wall corresponding to the combustor wall downstream of the injector, and the open right end of the 2-D flow corresponds to the open top of the injector. The height of the rectangular jet in the 2-D flow corresponds to the width of the injector in the 3-D flow.

In addition to geometry, fluid mechanical parameters are also matched: the light/heavy gas density ratio, and pressure and density jumps across the shocks are exactly the same: $\bar{\rho}_L/\bar{\rho}_H = 0.082$, $\bar{p}_2/\bar{p}_1 = 1.949$, and $\bar{\rho}_2/\bar{\rho}_1 = 1.597$.

Comparison of these plots shows good agreement between the flows, especially up to times $\bar{t}$=12 in the 2-D case. Beyond $\bar{t}$=12, small differences appear in the details of the flows, most notably at the downstream end of the 2-D structure and at the uppermost portion of the 3-D structure. This is most likely a consequence of the different amounts of dissipation in the two flows. The 3-D flow has higher viscous and diffusive terms, so its flow is much more smeared out, at late times, than the 2-D flow. Nevertheless, the general features are still fairly well correlated.

The 2-D and 3-D shock waves are shown schematically in Figures 15(a),(b). The corresponding equations for pressure and density jumps across the shock are given below.

2-D:

$$\frac{p_2}{p_1} = 1 + \frac{2\gamma_1}{\gamma_1 + 1}(M_{2-D}^2 - 1)$$

$$\frac{\rho_2}{\rho_1} = \frac{(\gamma_1 + 1)M_{2-D}^2}{(\gamma_1 - 1)M_{2-D}^2 + 2}$$

3-D:

$$M_{3-D}^2 = \frac{2cos(\beta - \delta)}{(sin\beta)[sin(2\beta - \delta) - \gamma_1 sin\delta]}$$

$$\frac{p_2}{p_1} = 1 + \frac{2\gamma_1}{\gamma_1 + 1}(M_{3-D}^2 sin^2\beta - 1)$$

$$\frac{\rho_2}{\rho_1} = \frac{(\gamma_1 + 1)M_{3-D}^2 sin^2\beta}{(\gamma_1 - 1)M_{3-D}^2 sin^2\beta + 2}$$

Correspondence of the pressure and density jumps requires that $M_{2-D} = M_{3-D}\ \sin\beta$, where β is determined from M_{3-D} and the turning angle δ. Quantitative comparison between the 2-D and 3-D flows requires the association of time in the 2-D unsteady flow with downstream distance in the 3-D steady flow. In that case, a velocity $(d\bar{x}/d\bar{t})_{2-D}$ may be related to a corresponding slope $(d\bar{z}/d\bar{x})_{3-D}$ by the simple relation

$$(d\bar{x}/d\bar{t})_{2-D} = m(d\bar{z}/d\bar{x})_{3-D},$$

where m is a conversion factor that is completely determined from the matching process: since the pressure and density jumps have been matched across the shock, consistency dictates that the motion of the shock be matched as well. Therefore, m must satisfy the relation

$$M_{2-D} = m\ tan(\beta - \delta)$$

or

$$m = \frac{M_{2-D}}{tan(\beta - \delta)}\ .$$

In the 2-D/3-D comparison shown earlier, M_{3-D} = 6 and $\delta = tan^{-1}(1/12)$, so that β = 0.2263 rad, M_{2-D} = 1.346, and m = 9.34. With m thus determined, one can compare the 2-D trajectory of the center of mass fraction and the 3-D jet lift-off. The computations give

$$(d\bar{x}/d\bar{t})_{2-D} = 0.18$$

and

$$(d\bar{z}/d\bar{x})_{3-D} = 0.017$$

so that

$$m(d\bar{z}/d\bar{x})_{3-D} = (9.34)(0.017) = 0.16.$$

The agreement between $(d\bar{x}/d\bar{t})_{2-D}$ and $m(d\bar{z}/\bar{x})_{3-D}$ is very good, indicating a trajectory correspondence in agreement with the matching of geometry, light/heavy gas density ratio, shock pressure jump, and shock density jump. Together with the observed qualitative agreement between the developing 2-D and 3-D structures, this reinforces the belief that the 2-D unsteady flow can be directly associated with a corresponding 3-D steady flow.

Conclusions

The canonical shock-induced vortical flow is the 2-D, unsteady passage of a shock wave over a single circular inhomogeneity ('jet') of light gas. Vorticity is generated baroclinically due to interaction of the pressure gradient from the shock wave and the density gradient at the light/heavy interface. This vorticity causes the jet to roll up and evolve toward a counterrotating vortex pair of finite core size. The vortex pair moves downstream relative to the ambient fluid due to the motion each vortex induces in the other. The circulation, velocity, and spacing of this vortex pair are essentially constant throughout the evolution of the flow.

The governing equations were integrated for various initial conditions, and the above flow variables were tabulated from these computations. Independently of the computations, closed-form analytical models were developed for the circulation, characteristic time of development, and normalized velocity. These models all agreed quite well with the computational results.

Various perturbations to the canonical flow were considered with the aim of enhancing the mixing of the light and heavy gases. Quantitative comparisons

were based on a stretching rate that is a necessary kinematical precursor of true molecular mixing. In general, the best mixing is achieved with strong shocks and low light/heavy gas density ratios. Also, the jets should be elongated normal to the shock, and should form arrays of closely spaced pairs, spaced far apart. Finally, reflected (or other multiple) shocks should be utilized, if possible, and the interaction should take place before the vortex pair formed by the incident shock has fully developed.

The above results were derived from studies of 2-D, unsteady flows, while real technological applications are more likely to be 3-D and steady. There exists an analogy between spatial development in the 3-D, steady flow and temporal development in the 2-D, unsteady flow that can be used to relate the two flows. This analogy was described mathematically, and used to construct an equivalent 2-D, unsteady flow corresponding to another investigator's computation of a particular 3-D, steady flow. The resulting flows agreed very well, both qualitatively and quantitatively.

Acknowledgements

This research was supported by the Air Force Office of Scientific Research, under the supervision of Dr. Julian Tishkoff, through contract number F49620-86-C-0113 and grant number AFOSR-90-0188. It was also supported by the National Science Foundation through a Cray supercomputer grant at the San Diego Supercomputer Center. The first author was supported by the Office of Naval Research through an ONR Graduate Fellowship. The authors would like to thank Dr. Elaine S. Oran, of the Laboratory for Computational Physics at the Naval Research Laboratory, for providing the algorithm used in the numerical simulations.

References

1) Batchelor, G. K. (1952), "The Effect of Homogeneous Turbulence on Material Lines and Surfaces," Proc. Roy. Soc. London 213A, pp. 349-366.

2) Hendricks, G. J. and Marble, F. E. (1991), "Shock Enhancement of Supersonic Combustion Processes," Preliminary draft of a manuscript in preparation.

3) Leonard, A. (1991), Personal communication.

4) Marble, F. E., Hendricks, G. J., and Zukoski, E. E. (1987) "Progress toward Shock Enhancement of Supersonic Combustion Processes," AIAA Paper 87-1880.

5) Marble, F. E., Zukoski, E. E., Jacobs, J. W., Hendricks, G. J., and Waitz, I. A. (1990), "Shock Enhancement and Control of Hypersonic Mixing and Combustion," AIAA Paper 90-1981.

6) Oran, E. S. (1991), "LCPFCT - A Monotone Algorithm for Solving Continuity Equations," Preliminary draft of a manuscript in preparation.

7) Picone, J. M. and Boris, J. P. (1988), "Vorticity Generation by Shock Propagation Through Bubbles in a Gas," J. Fluid Mech. 189, pp. 23-51.

8) Picone, J. M., Oran, E.S., Boris, J. P. and Young, T. R. (1985), "Theory of Vorticity Generation by Shock Wave and Flame Interactions," in Dynamics of Shock Waves, Explosions, and Detonations, AIAA, pp. 429-448.

9) Rudinger, G. and Somers, L. M. (1960), "Behaviour of Small Regions of Different Gases Carried in Accelerated Gas Flows," J. Fluid Mech. 7, pp. 161-176.

10) Waitz, I. A. (1991) "A Contoured Wall Injector for Hypervelocity Mixing Augmentation," Ph.D. Thesis, California Institute of Technology.

11) Yang, J., "An Analytical and Computational Investigation of Shock-Induced Vortical Flows," Ph.D. Thesis, California Institute of Technology, 1991.

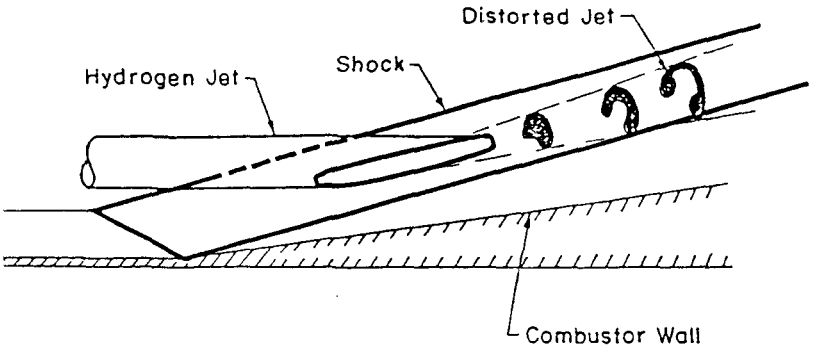

Figure 1 - 3-D, Steady Shock-Induced Mixing [Reproduced from Ref. 5 with permission]

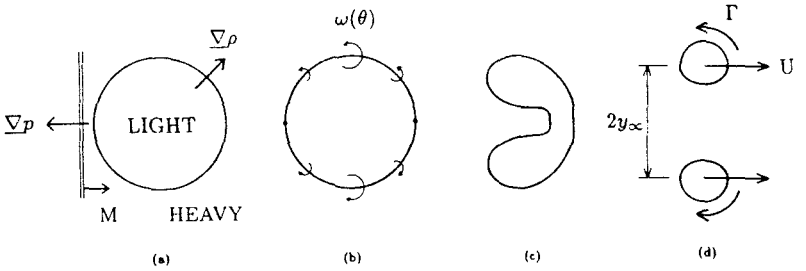

Figure 2 - 2-D, Unsteady Shock-Induced Mixing

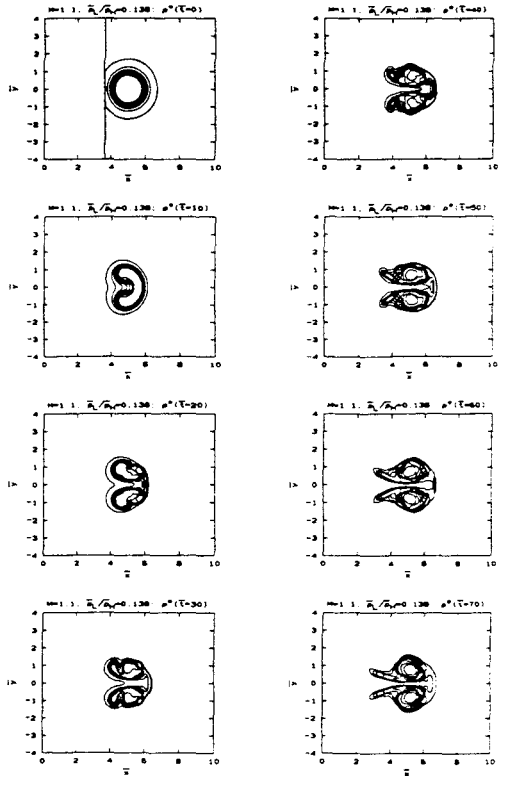

Figure 3 - M=1.1, $\overline{\rho}_L/\overline{\rho}_H = 0.138$ Canonical Flow

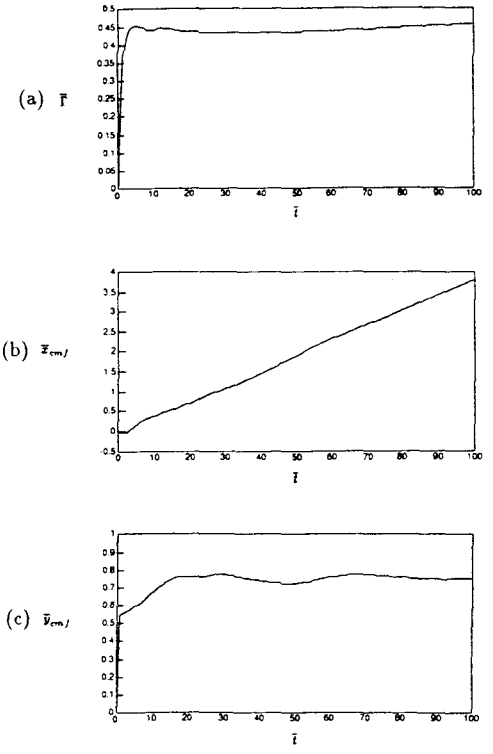

Figure 4 - $\overline{\Gamma}$, $\overline{x}_{cmf}$, *and* $\overline{y}_{cmf}$ for Figure 3

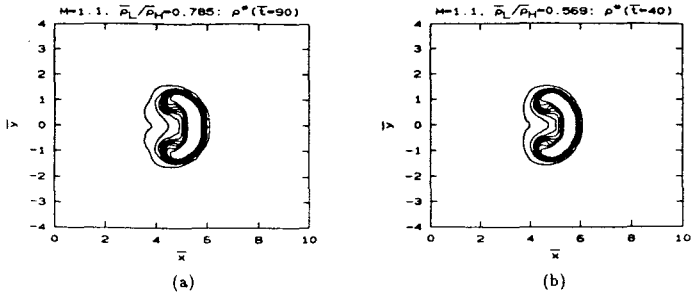

Figure 5 - Time Scaling Comparison

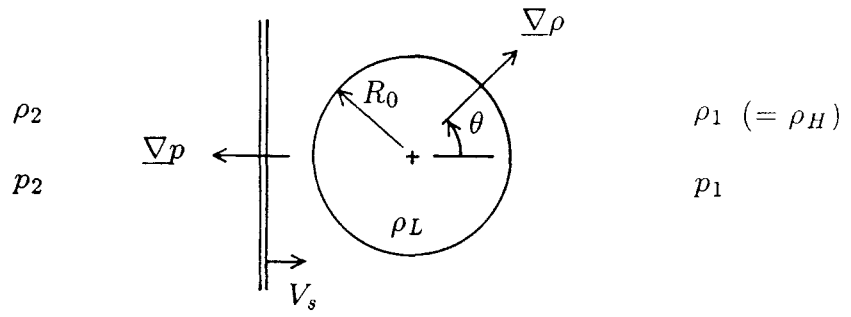

Figure 6 - Schematic for $\overline{\Gamma}$ Calculation

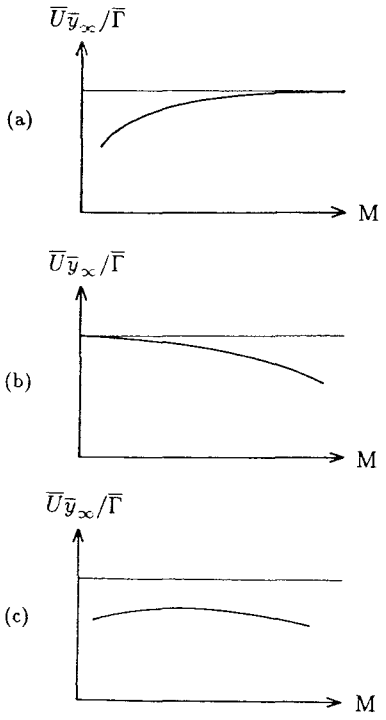

Figure 7 - $\overline{U}\overline{y}_\infty/\Gamma$ for fixed $\overline{\rho}_L/\overline{\rho}_H$

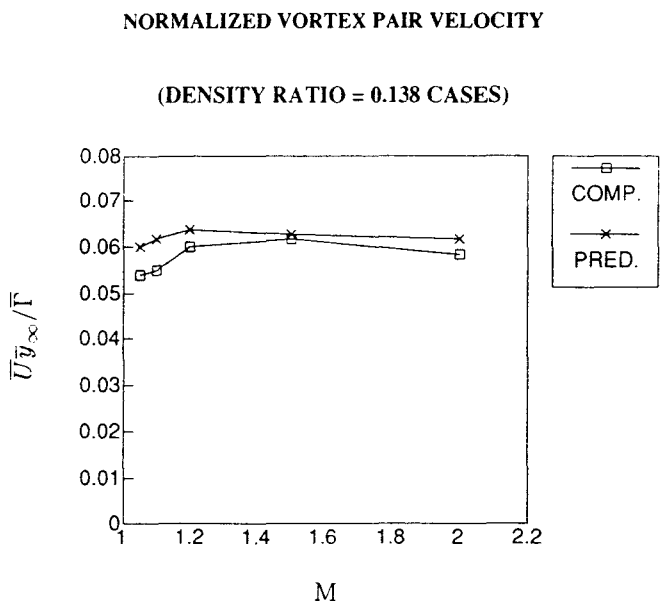

Figure 8 - $\overline{U}\overline{y}_\infty/\Gamma$ for $\overline{\rho}_L/\overline{\rho}_H = 0.138$

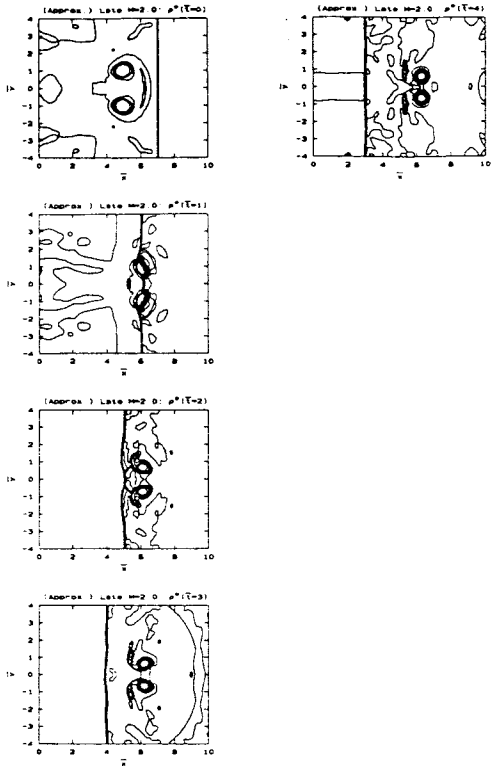

Figure 9 - Late-time Reflected Shock

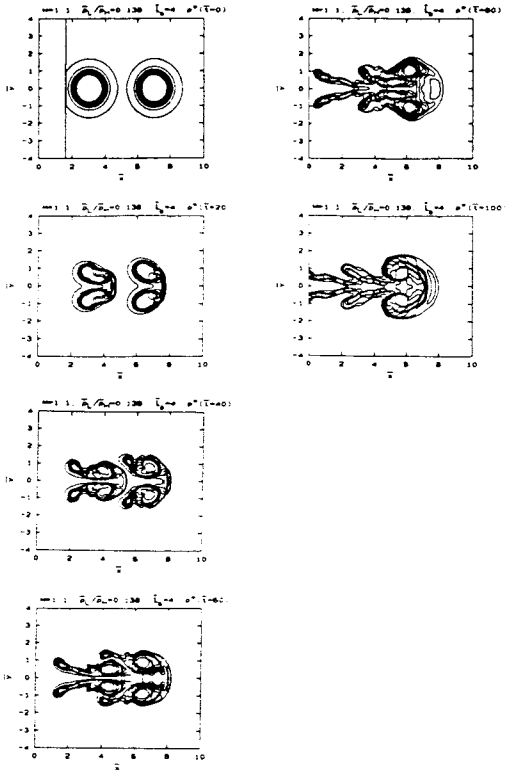

Figure 10 - Horizontal Jet Pair

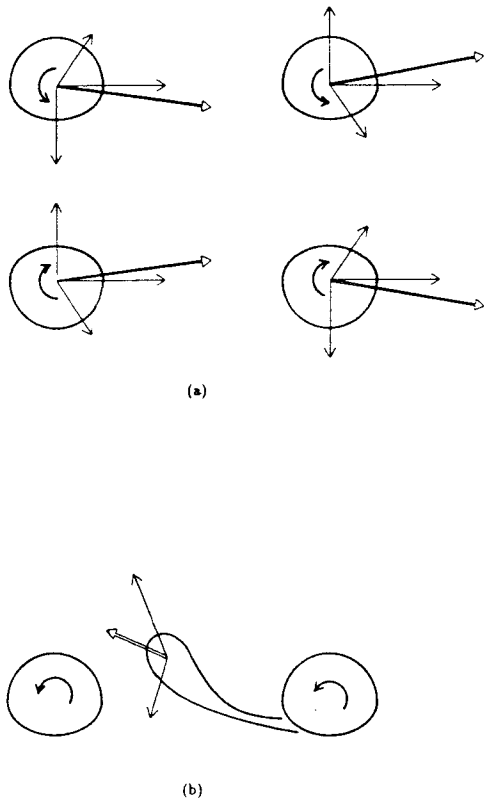

Figure 11 - Horizontal Jet Pair Induced Motions

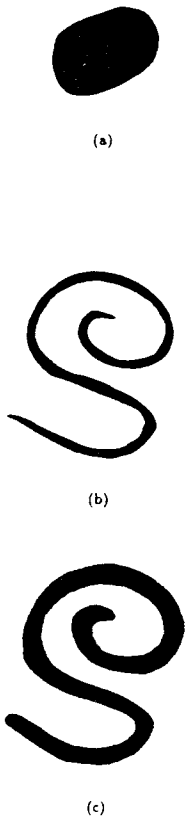

Figure 12 - Mixing Schematic

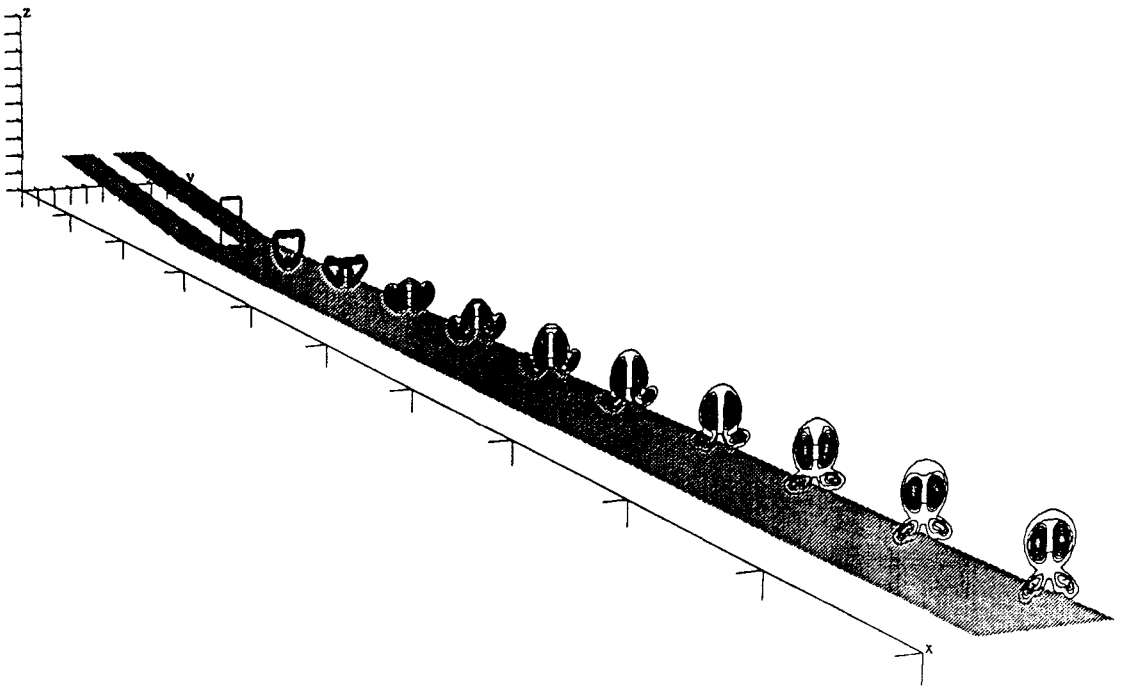

Figure 13 - Waitz's 3-D Steady Computation [Reproduced from Ref. 10 with permission]

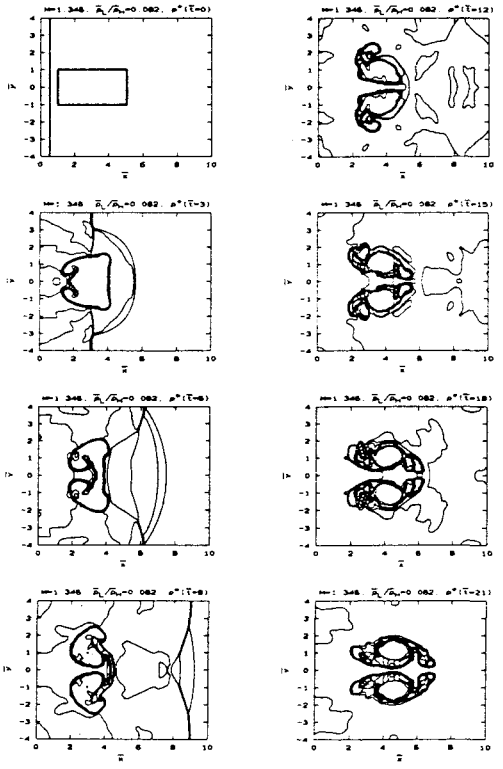

Figure 14 - 2-D, Unsteady Equivalent of Figure 13

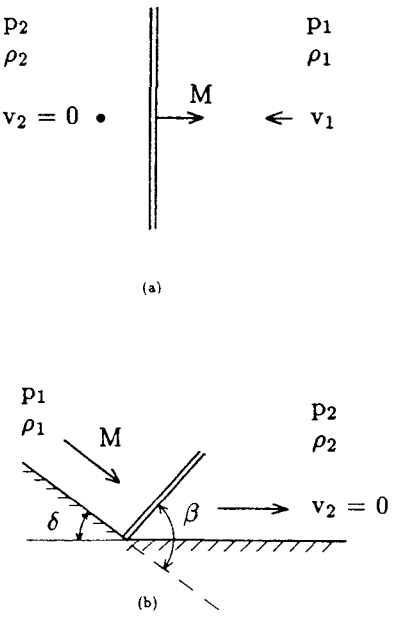

Figure 15 - Schematic for 2-D/3-D Analogy